J. Fluid Mech. (1996), *vol.* 329, *pp.* 137–146

Numerical investigation of the dynamic influence of the contact line region on the macroscopic meniscus shape

By IVAN B. BAZHLEKOV[1] AND ALLAN K. CHESTERS[2]†

[1] Institute of Mathematics, BAS, acad. G. Bonchev str. bl. 8, 1113 Sofia, PO Box 373, Bulgaria

[2] Laboratory of Fluid Dynamics and Heat Transfer, Eindhoven University of Technology, PO Box 513, Eindhoven, The Netherlands

(Received 25 July 1994 and in revised form 1 July 1996)

The influence of different boundary conditions applied in the contact line region on the outer meniscus shape is analysed by means of a finite-element numerical simulation of the steady movement of a liquid–gas meniscus in a capillary tube. The free-surface steady shape is obtained by solving the unsteady creeping-flow approximation of the Navier–Stokes equations starting from some initial shape. Comparisons of the outer solutions obtained using two different inner models, together with that published by Lowndes (1980), indicate the relative insensitivity of the outer solution to the type of model utilized in the contact line region.

1. Introduction

The dynamics of the three-phase contact region, in which a liquid–fluid interface joins a solid surface, determines the wetting/de-wetting of the solid in response to applied constraints. From a macroscopic point of view, the hydrodynamics of such processes is determined by the relation between the wetting speed and the (apparent) dynamic contact angle, Φ_d. While for smooth homogeneous solids the static contact angle, Φ_s, depends only on the materials involved (extremely small systems excepted), Φ_d is dependent both on the wetting speed and (more weakly) on the system scale/geometry (Kafka & Dussan V. 1979).

The first attempts to understand why Φ_d differs from Φ_s were based on an analysis of the (creeping) flow generated by displacement of the contact line, which gives rise to pressure variations tending to deform the meniscus in a microscopic region close to the line, thereby increasing the apparent contact angle in the advancing fluid. This prediction has recently been confirmed experimentally, the meniscus curvature increasing continually as the contact line is approached, up to the limit of observation of less than 10^{-7} m from the solid (van der Zanden & Chesters 1994*a*).

While the confirmation that Φ_d is an apparent rather than true contact angle is reassuring, two obstacles to a complete model for $\Phi_d - \Phi_s$ remain. The first is that the above hydrodynamic effect may be imposed on a genuine wetting-speed dependence of the true contact angle, Φ_0 (the limiting meniscus inclination at distances from the solid of the order of a molecular dimension). The second is that if the classical approximations of fluid mechanics are retained, the predicted magnitude of $\Phi_d - \Phi_0$ is infinite for all wetting speeds – in clear contrast with observation. The origin of this

† Author to whom correspondence should be addressed.

problem lies in a stress singularity at the contact line which disappears only if one or more of these classical approximations is supposed to fail.

Various possibilities have been suggested: breakdown of the no-slip approximation at the solid (Huh & Mason 1977; Lowndes 1980; and others), breakdown of the representation of inter-molecular forces solely by an interfacial tension (de Gennes, Hua & Levinson 1990; Kalliadasis & Chang 1994) and breakdown of the continuum description itself (Boender, Chesters & van der Zanden 1991). Each of these hypotheses leads to an inner length scale, l, which, together with the true contact angle, determines the meniscus shape in the outer region, where the classical approximations apply. The values of l obtained from comparing the resulting models with experimental data suggest that l is typically of the order of a molecular dimension ($l \sim 10^{-9}$ m: Lowndes; Boender *et al.*; van der Zanden & Chesters 1994*a*).

A full resolution of the mechanics of the inner, non-classical region, including any difference between Φ_0 and Φ_s, can probably be provided only by molecular-dynamics simulations. As such approaches are at present in their infancy, being able to cope only with very small systems and simple interaction potentials (Koplik, Banavar & Willemsen 1989), a practically important question is how essential a detailed understanding of the inner region is to the description of the outer region (in particular, the value of Φ_d). Specifically, given a meniscus inclination Φ_λ at some distance λ from the wall, how does the solution at distances greater than λ depend on the inner model adopted?

The present paper addresses this question by deriving finite-element solutions for the meniscus shape associated with a steadily advancing viscous liquid in a capillary tube for two different inner boundary conditions: a slip condition as used by Shopov & Bazhlekov (1991) and the continuum-breakdown model of Boender *et al.* The comparisons also include the finite-element results of Lowndes, who used a slightly different slip condition.

It is intuitively clear, as proposed by Kafka & Dussan V. (1979), that for given Φ_λ the dependence of the outer solution on the inner model will be weak for λ-values satisfying

$$1 \ll \lambda \ll a, \tag{1}$$

where a denotes the tube radius. The main interest here concerns how small λ can become before the influence of the inner model becomes significant. Specifically, should the lower λ-limit prove to be of the order of the inner length scale, l, which itself is of the order of a molecular dimension, then Φ_λ can be equated with the true contact angle, Φ_0, reducing the modelling task to a description of the velocity dependence of Φ_0.

Section 2 develops the equations to be solved, including the boundary conditions associated with the three inner models. The finite-element method is outlined in §3 and the results presented in §4. The final section examines their implications – in particular, in regard to the original question of how essential a complete understanding of the inner dynamics is to a description of the outer region.

2. Mathematical formulation of the problem

2.1. *The outer region: continuum equations and boundary conditions*

Consider the movement of a liquid displacing gas with a constant velocity U in a smooth capillary tube of radius, a, small enough for the influence of gravity on the flow to be neglected. If the inflow at some distance from the meniscus is axisymmetric with respect the tube centreline the problem can be considered as a two-dimensional

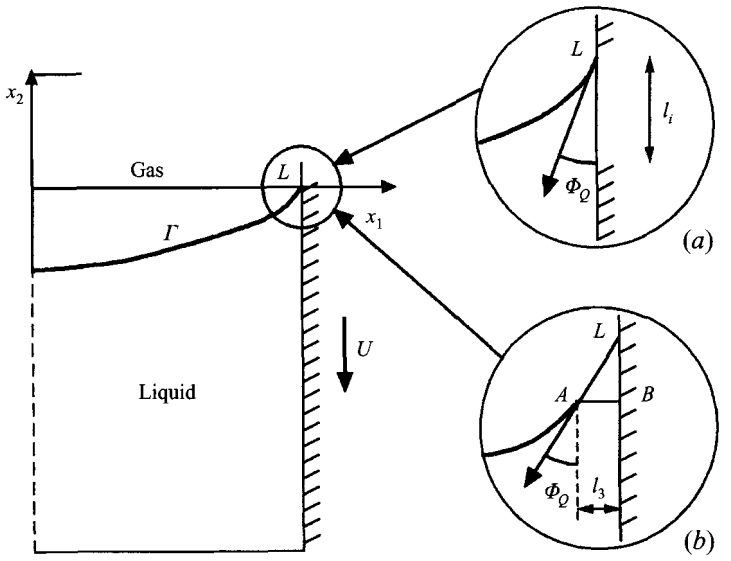

FIGURE 1. Schematic of the steady motion of a meniscus in a capillary tube: (*a*) for inner boundary conditions B1 and B2; (*b*) for inner boundary condition B3.

axisymmetric one. The cylindrical coordinate system (x_1, x_2) moving with the contact line (see figure 1) is chosen as a reference frame. It is also assumed that the liquid is incompressible and Newtonian and that inertial forces are negligible, i.e. Reynolds number $Re = \rho a U/\mu \ll 1$, where ρ is the density and μ is the dynamic viscosity of the liquid. Choosing μ, a, and the wall velocity, U, as reference quantities the creeping-flow approximation of the Navier–Stokes equation governing the liquid motion in the outer region can be written in dimensionless form as

$$\nabla \cdot \boldsymbol{\Pi} = 0, \tag{2}$$

where $\boldsymbol{\Pi}$ is the stress tensor with components

$$\Pi_{ij} = -p\delta_{ij} + (u_{i,j} + u_{j,i}), \tag{3}$$

p is the dimensionless pressure in the liquid and $\boldsymbol{u} = (u_1, u_2)$ is the velocity.

The continuity equation is

$$\nabla \cdot \boldsymbol{u} = 0. \tag{4}$$

The boundary conditions to the above system of differential equations are as follows:

(*a*) Balance of the stress and the capillary pressure on the free surface Γ defined by the equation $x_2 = h(x_1)$:

$$-\boldsymbol{\Pi} \cdot \boldsymbol{n} - p_g \boldsymbol{n} = \boldsymbol{n}(R_1^{-1} + R_2^{-1})/Ca, \tag{5}$$

where $\boldsymbol{n}$ is a normal to Γ, p_g is pressure in the gas phase, which is assumed to be constant, R_1 and R_2 are the principal radii of curvature of Γ (R_i is reckoned positive if its centre of curvature lies on the liquid side).

(*b*) Vanishing normal component of the velocity on the free surface Γ:

$$\boldsymbol{u} \cdot \boldsymbol{n} = 0 \quad \text{on} \quad x_2 = h(x_1). \tag{6}$$

(*c*) At the tube centreline $x_1 = 0$:

vanishing normal velocity:

$$u_1 = 0; \tag{7}$$

vanishing tangential stress:

$$\Pi_{12} = 0. \tag{8}$$

(*d*) Analytical (Huh & Mason 1977), numerical (Lowndes 1980) and experimental (Hoffman 1975) results suggest that the computational flow domain need only extend a distance of one tube diameter from the meniscus position. So two alternative upstream boundary conditions at dimensionless distance 2.5 from the contact line ($x_2 = -2.5$) were used:

(i) vanishing radial velocity component and axial component of the axial velocity gradient:

$$u_1 = 0, \quad u_{2,2} = 0 \quad \text{at} \quad x_2 = -2.5; \tag{9a}$$

(ii) Poiseuille flow:

$$u_1 = 0, \quad u_2(x_1) = -2x_1^2 + 1 \quad \text{at} \quad x_2 = -2.5, \tag{9b}$$

defined by the equations

$$u_2(1) = -1; \quad u_{2,1}(0) = 0, \quad \int_0^1 x_1 u_2(x_1)\,\mathrm{d}x_1 = 0.$$

The meniscus profiles obtained using upstream boundary conditions (9*a*) or (9*b*) are identical. This suggests that the solution is independent of the form chosen as well as of any additional extension of the computational domain (to more than 2.5 radii).

(*e*) At the tube wall $x_1 = 1$, the impermeability condition:

$$u_1 = 0. \tag{10}$$

2.2. *Boundary conditions imposed by the inner region*

Three types of inner boundary condition are explored:

B1: Solution of the flow over the entire liquid domain Ω, supposing slip between wall and adjacent liquid up to a distance l_1 from the contact line L, given by

$$u_2 = x_2/l_1 \quad \{-l_1 \leqslant x_2 \leqslant 0; x_1 = 1\}, \tag{11a}$$

$$u_2 = -1 \quad \{x_2 \leqslant -l_1; x_1 = 1\}, \tag{11b}$$

corresponding to linear variation of the slip velocity up to a distance l_1 from the contact line L (see figure 1*a*).

B2: Solution over the entire domain Ω, supposing slip at the solid surface described by a linear relation between shear stress and slip velocity (Navier slip condition):

$$\Pi_{12} = -2/l_2(1 + u_2(x_2)) \quad \text{on} \quad x_1 = 1. \tag{12}$$

B3: Solution over the domain below the segment AB of length l_3 (see figure 1*b*), applying the no-slip condition at the wall and taking as condition on the boundary AB Moffatt's (1964) analytical solution for the flow in the plane wedge ALB.

The condition B2 is that utilized by Lowndes, who obtained good correspondence with macroscopic observations of the meniscus form (apparent contact angle) taking the angle Φ_Q in figure 1(*a*) equal to Φ_s and l_2 of the order of 10^{-9} m. The slip resulting from this boundary condition is significant over a distance of order l_2, being maximal at the contact line and becoming negligible when $-x_2 \gg l_2$.

A qualitatively similar variation of the slip velocity is imposed by the condition B1,

which is that utilized by Shopov & Bazhlekov, the slip velocity varying linearly from its maximum value at the contact line to zero at $-x_2 = l_1$ (corresponding with the mid-point on the base of the first finite element). In this case, a non-physical discontinuity is introduced in the velocity gradient at the point $-x_2 = l_1$, which however presents no computational difficulties.

The condition B3 corresponds to that used by Boender *et al.*, who derived an approximate equation for the meniscus inclination, $\Phi(x_1)$, based on Moffatt's plane-wedge solution which respects the no-slip condition (Moffatt 1964). The transition from the continuum domain in which this equation is applicable to the last few molecular layers in which the final inclination, Φ_0, is attained, was approximated as occurring abruptly at a distance from the solid, l_3, of the order of a molecular dimension. In addition to the boundary conditions of no slip and of specified meniscus inclination, Φ_Q (figure 1*b*) at distance l_3 from the solid, it is necessary for the finite-element solution to specify conditions on the boundary segment AB. The choice made here – of conditions on AB corresponding to Moffatt's solution in the plane wedge ALB – is the simplest option compatible with the other boundary conditions.

To determine the meniscus shape in the cases B1–B3 the inclination Φ_Q has to be specified at some point Q:

$$\boldsymbol{n}\cdot\boldsymbol{n}_{W|Q} = \cos(\Phi_Q), \tag{13}$$

where $\boldsymbol{n}_W$ is the unit normal to the wall $\boldsymbol{n}_W = (-1, 0)$ and $\boldsymbol{n}$ is the unit normal to the free surface. Q is chosen as the point L for cases B1 and B2 and as the point A for case B3 respectively (see figure 1*a*, *b*). Thus the problem described above depends on Ca – capillary number, l_1 or l_2 – dimensionless slip lengths in cases B1 and B2 respectively and length l_3 of the segment AB in case B3 and the 'contact angle' Φ_Q.

3. Numerical formulation

The mathematical problem described in the previous section is solved by means of a finite-element method developed to cope with both steady and unsteady wetting problems. The principles and advantages of the application of finite-element methods to capillary motion problems have been well described by Lowndes (1980) (see also references therein). The finite-element method used in the present paper is of the divergence-free type in velocity–pressure variables. The elements are isoparametric quadrilaterals with 9-node biquadratic approximations $\{\phi^i\}$ for velocity and bilinear ones $\{\psi^i\}$ for pressure on a standard (ξ, η) square domain. As the method is described in detail in Shopov, Minev & Bazhlekov (1990) and Shopov & Bazhlekov (1991), only a brief description of the numerical scheme is presented in the present section, emphasizing the determination of the steady meniscus position and the prescription of the meniscus inclination Φ_Q (condition (13)).

The solution for velocity and pressure is determined by requiring that the Galerkin weighted residuals of momentum and continuity vanish:

$$\int_\Omega \boldsymbol{\Pi}\cdot\nabla\phi^i \,\mathrm{d}\Omega - \int_{\partial\Omega} \boldsymbol{n}\cdot\boldsymbol{\Pi}\phi^i \,\mathrm{d}s = 0, \tag{14}$$

$$\int_\Omega \nabla\cdot\boldsymbol{u}\psi^k \,\mathrm{d}\Omega = 0, \tag{15}$$

where the velocity $\boldsymbol{u}$ and pressure p are presented by

$$\boldsymbol{u} = \sum \boldsymbol{u}^i\phi^i, \quad p = \sum p^k\psi^k. \tag{16}$$

The essential boundary conditions (7), (9*b*) and (10)–(11), as well as inner condition B1, are imposed by replacing the equations for the particular degrees of freedom by equations enforcing these conditions. The natural boundary conditions (5), (8) and (9*a*) are imposed through the boundary integral in (14), which takes the form

$$\int_{\Omega} -\boldsymbol{\Pi}\cdot\nabla\phi^i \,\mathrm{d}\Omega - \frac{1}{Ca}\int_{\Gamma} n(R_1^{-1}+R_2^{-1})\,\phi^i \,\mathrm{d}s + \frac{1}{Ca}(\boldsymbol{n}\cdot\boldsymbol{n}_{W|Q} - \cos\Phi_Q)\,\boldsymbol{\tau}_W\,\phi^i(Q) = 0, \quad (17)$$

where $\boldsymbol{n}$ is the unit normal to Γ and $\boldsymbol{n}_W$ and $\boldsymbol{\tau}_W$ are the unit normal and tangential vectors to the solid surface.

The last term in (17) is due to shell forces at the contact line (see Christodoulou & Scriven 1989). From a numerical point of view it is a penalty function which keeps the inclination at point Q equal to the prescribed value Φ_Q. As noted, the point Q is the contact-line point L in cases B1 and B2 and the point A in case B3. Thus making the size of the finite elements in the vicinity of point Q go to zero the contribution of both integrals in (17) at point Q will also go to zero, i.e. $\boldsymbol{n}\cdot\boldsymbol{n}_{W|Q}\to\cos(\Phi_Q)$. This is the case since the elements of the stress tensor $\boldsymbol{\Pi}$ are bounded at Q and the diameter of the support of the basic function ϕ^i decreases with decreasing element size. The finite-element size in the vicinity of point Q is therefore chosen small enough for the condition (13) to be satisfied with some required accuracy. For the results presented in the present paper the deviation of the inclination obtained from that required by (13) is less than 0.01°. Thus (13) is satisfied in a natural way and the velocity and pressure fields obtained satisfy the whole mathematical formulation (2)–(13) except for (6).

To obtain the steady meniscus position $\Gamma: x_2 = h(x_1)$ the unsteady problem is solved, beginning from an initial configuration Γ_0 and using the standard kinematic condition for $\Gamma(t): x_2(t) = h(x_1, t)$

$$\frac{\partial h(x_1, t)}{\partial t} = \boldsymbol{n}(t)\cdot\boldsymbol{u}(t), \quad (18)$$

where $\boldsymbol{n}(t)$ is the normal to Γ defined by $\boldsymbol{n}(t) = (-\partial h(x_1, t)/\partial x_1; 1)$.

Applying an explicit scheme to the left-hand side of (18) and knowing the meniscus position at time t: $x_2(t) = h(x_1, t)$ and the velocity field $\boldsymbol{u}(t) = (u_1(t), u_2(t))$ the meniscus position at instant Δt later can be computed with error $O(\Delta t^2)$ from

$$h(x_1, t+\Delta t) = h(x_1, t) + \Delta t\boldsymbol{n}(x_1, h(x_1, t), t)\cdot\boldsymbol{u}(x_1, h(x_1, t), t). \quad (19)$$

The steady position Γ, then, is the limit of $\Gamma(t)$ as $t\to\infty$, i.e. $h(x_1) = \lim_{t\to\infty} h(x_1, t)$. In practice the calculation is stopped when $\boldsymbol{n}(x_1, t)\cdot\boldsymbol{u}(x_1, t)$ becomes small enough and the meniscus hardly moves anymore. The steady meniscus shapes presented here satisfy the requirement $\boldsymbol{n}\cdot\boldsymbol{u} < 0.01$, i.e. the boundary condition (6) is satisfied within an error of less than 0.01.

The advantage of the above described numerical scheme, compared with available ones, consists in its applicability to unsteady problems. However, for steady ones it requires more computational time than that used by Lowndes (1980). The reason is that the maximum value of Δt is limited by numerical instability and decreases with decreasing element size and capillary number, becoming prohibitively small for elements of the required (subnanometer) size in the neighbourhood of point Q. To circumvent this problem, only the elements immediately adjacent to the interface are addressed at each time step, a full calculation being performed intermittently. It should be noted that this approach does not introduce any additional errors as the

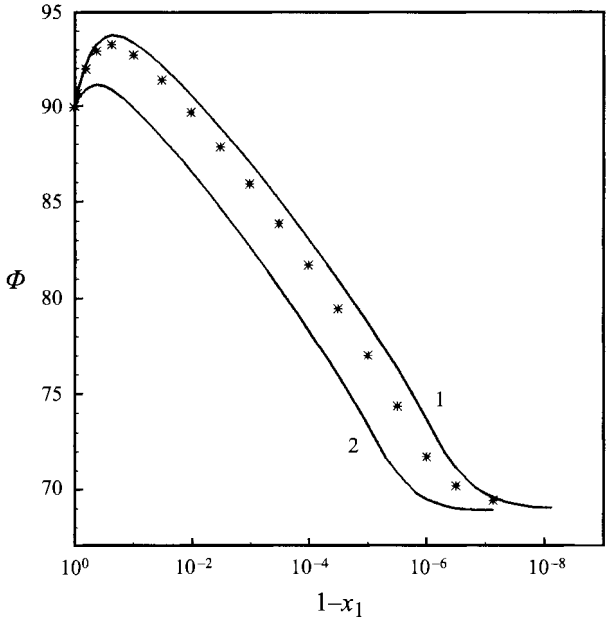

FIGURE 2. The inclination, $\Phi(x_1)$, of the meniscus profile obtained using the inner boundary condition B1 at three different slip lengths (m): curve 1, 10^{-9}; *, 3×10^{-9}; curve 2, 10^{-8}. $Ca = 0.0211$, $\Phi_Q = 69°$.

displacement of the interface changes only the adjacent elements and their local matrices. Optimization of this approach resulted in a reduction of the computational time by an order of magnitude, enabling the required resolution to be attained.

In order to optimize the number of finite elements used and to present the solution adequately logarithmically decreasing mesh sizes were used near the contact line (point Q) (see those used by Lowndes). The dimensionless spatial step in the vicinity of Q is chosen of order 10^{-9}. This step guarantees a good approximation of the conditions (5), (11), (13) as well as the inner boundary condition B3 in the range of parameters considered.

4. Results

Figure 2 presents the results of computations using the boundary condition B1 with three different values of the dimensionless inner length, l_1. The values of Ca and Φ_Q correspond to the Ca- and Φ_s-values in one of the cases investigated experimentally by Hoffman (1975), using a capillary tube of radius 0.978 mm. The numerical results indicate that the outer solution is fairly sensitive to the value of the inner length scale, a conclusion also reached by Lowndes, who employed the boundary condition B2 in his finite-element solution, and by Boender *et al.* using an analytical approximation employing the boundary condition B3. Both Lowndes and Boender *et al.* obtained optimal agreement with the Hoffman's experimental results (Φ_d-values) using an inner length scale of around 10^{-9} m and this value is adopted for all three boundary conditions in what follows.

Figure 3(*a*) displays the computed variation of the meniscus inclination Φ with dimensionless distance from the wall, $1 - x_1$, using the boundary conditions B1–B3, for the same values of Φ_Q and Ca as in figure 2. Curves 1 and 3 correspond to the boundary conditions B1 and B3 respectively, while the circles represent the results obtained by

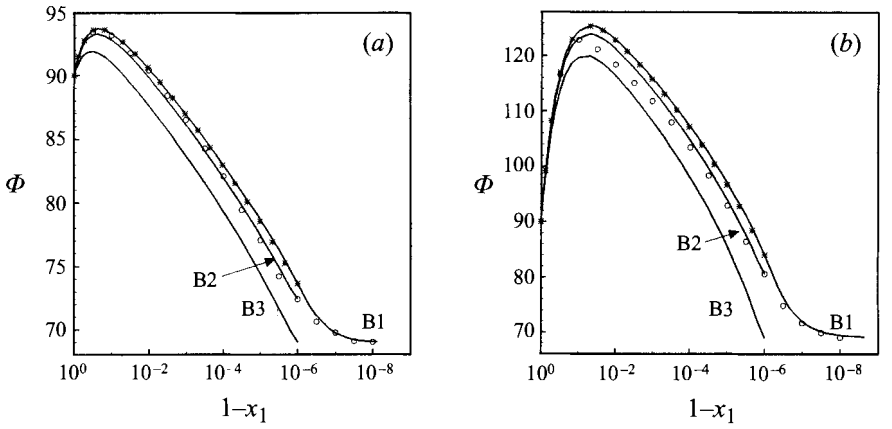

FIGURE 3. Comparison between different inner models for $\Phi_Q = 69°$ and l_i (dimensionless) $= 10^{-6}$: (*a*) $Ca = 0.0211$; (*b*) $Ca = 0.0753$.

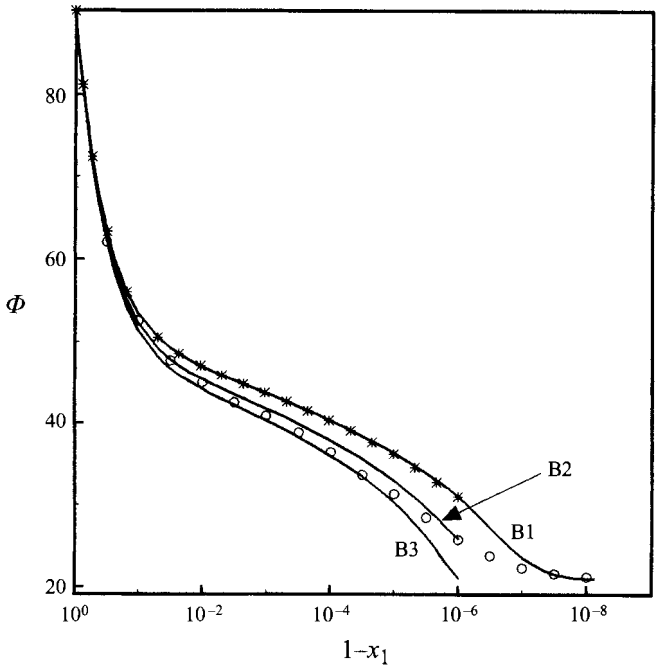

FIGURE 4. Comparison between different inner models for $\Phi_Q = 21°$, l_i (dimensionless) $= 10^{-6}$ and $Ca = 0.00428$.

Lowndes, using condition B2. A small error – probably 0.5° or less – is introduced in converting Lowndes' results, which were presented as plots of the meniscus slope ($\cot\Phi$), into Φ-values. The corresponding results for a higher Ca-value are given in figure 3(*b*), while figure 4 presents those for one of the cases examined experimentally by Hansen & Toong (1971) using a capillary of 1.19 mm radius. The differences between the three solutions are marked.

The values of Φ obtained at distance 10^{-9} m from the wall ($1-x_1 \approx 10^{-6}$) using boundary condition B1 were now taken as Φ_Q-values for a new computation using boundary condition B3. The resulting points (*) in figures 3 and 4 are seen to lie almost

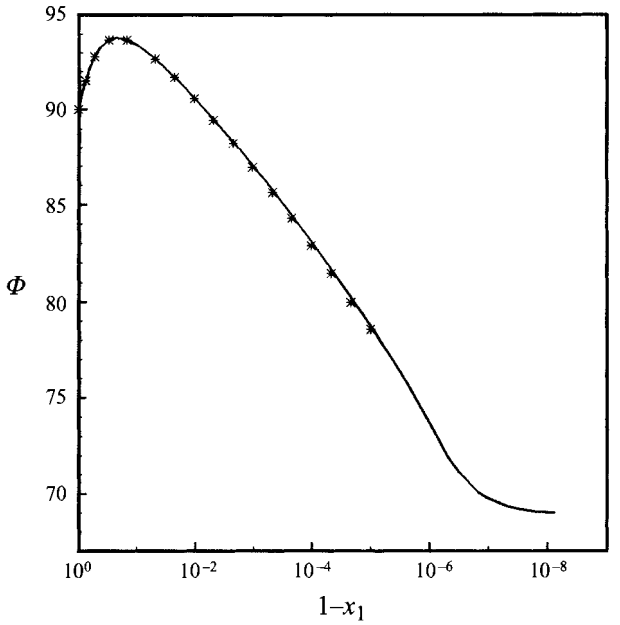

FIGURE 5. Comparison between solutions obtained at $Ca = 0.0211$ using the inner boundary condition B1 for $l_1 = 10^{-6}$ and $\Phi_Q = 69°$ (the line) and that using B3 with $l_3 = 10l_1$ and Φ_Q taken from the B1-solution (points).

perfectly on curve 1, indicating that for a λ-value equal to the inner length scale the outer solution is already virtually independent of the inner boundary condition used. As would be expected, this behaviour is maintained for larger λ-values: figure 5.

In contrast, the same procedure for boundary condition B2 yielded curve 2, which corresponds less satisfactorily with the circles. As conditions B1 and B2 are alike (both being slip conditions), it seems likely that this lack of correspondence is primarily due to numerical inaccuracies in one or both of the finite-element schemes (the present method and that of Lowndes). Such inaccuracies would not show up in the comparison between curve 1 and the * points, as they would contribute in the same way to both.

5. Discussion

Returning to the issues set out in the Introduction, a number of conclusions can now be drawn. The first is that the results corroborate the proposal of Kafka & Dussan V. (1979) that for given meniscus inclination at distance λ from the wall, the meniscus shape at greater distances is independent of the inner model and boundary conditions, provided λ satisfies (1).

More importantly, for the slip and continuum-breakdown models numerically investigated here, the smallest value of λ exhibiting this independence is of the order of the inner length scale, l, itself, so that the meniscus shape follows from the value of $\Phi(l)$, regardless of the inner model. Estimates of l (for either type of model) being of the order of a molecular dimension for the systems investigated to date, the tentative conclusion is then that $\Phi(l)$ can be equated with the true contact angle Φ_0, which constitutes a sufficient boundary condition for the outer, classical region.

This conclusion is of course at present limited to the case examined here of a viscous liquid steadily displacing a gas from a smooth homogeneous solid and even then there

may be an exception for systems exhibiting a very small (but non-zero) static contact angle, when the inner length scale should be greater than a molecular dimension as a result of the dominant influence of van der Waals interactions (de Gennes *et al.* 1990). Nevertheless, as there are no obvious physical grounds for expecting the inner length scales to be of a different order in receding, gas–liquid or liquid–liquid systems, the present simplifications probably apply there too. Unlike the advancing case, the predicted wetting behaviour is then highly sensitive to the value of Φ_0 and present indications are that its value often depends significantly on the wetting speed (Chesters & van der Zanden 1993; Zhou & Sheng 1990; van der Zanden & Chesters 1994*b*).

This work was carried out while I. B. Bazhlekov was a fellow at Eindhoven University of Technology under the European-Community scheme S&T Cooperation with Eastern and Central European Countries and was further sponsored by grant no. 501/95 of the Bulgarian Ministry of Education, Science and Technology.

REFERENCES

BOENDER, W., CHESTERS, A. K. & ZANDEN, A. J. J. VAN DER 1991 An approximate analytical solution of the hydrodynamic problem associated with an advancing liquid–gas contact line. *Intl J. Multiphase Flow* **17**, 661.

CHESTERS, A. K. & ZANDEN, A. J. J. VAN DER 1993 An approximate solution of the hydrodynamic problem associated with receding liquid-gas contact lines. *Intl J. Multiphase Flow* **19**, 905.

CHRISTODOULOU, K. N. & SCRIVEN, L. E. 1989 The fluid mechanics of slide coating. *J. Fluid Mech.* **208**, 321.

GENNES, P. G. DE, HUA, X. & LEVINSON, P. 1990 Dynamics of wetting: local contact angles. *J. Fluid Mech.* **212**, 55.

HANSEN, R. J. & TOONG, T. Y. 1971 Interface behavior as one fluid completely displaces another from a small-diameter tube. *J. Colloid Interface Sci.* **36**, 410.

HOFFMAN, R. 1975 A study of the advancing interface. I. Interface shape in liquid-gas systems. *J. Colloid Interface Sci.* **50**, 228.

HUH, C. & MASON, S. G. 1977 The steady movement of a liquid meniscus in a capillary tube. *J. Fluid Mech.* **81**, 401.

KAFKA, F. Y. & DUSSAN, V., E. B. 1979 On the interpretation of dynamic contact angles in capillaries. *J. Fluid Mech.* **95**, 539.

KALLIADASIS, S. & CHANG, C.-H. 1994 Apparent dynamic contact angle of an advancing gas-liquid meniscus. *Phys. Fluids* **6**, 12.

KOPLIK, J., BANAVAR, J. R. & WILLEMSEN, J. F. 1989 Molecular dynamics of fluid flow at solid surfaces. *Phys. Fluids* A **1**, 781.

LOWNDES, J. 1980 The numerical simulation of the steady motion of the fluid meniscus in a capillary tube. *J. Fluid Mech.* **101**, 631.

MOFFATT, H. K. 1964 Viscous and resistive eddies near a sharp corner. *J. Fluid Mech.* **18**, 1.

SHOPOV, P. J. & BAZHLEKOV, I. B. 1991 Numerical method for viscous hydrodynamic problems with dynamic contact lines. *Comput. Meth. Appl. Mech. Engng* **91**, 1157.

SHOPOV, P. J., MINEV, P. D. & BAZHLEKOV, I. B. 1992 Numerical method for unsteady viscous hydrodynamical problem with free boundaries. *Intl J. Numer. Meth. Fluids* **14**, 681.

ZANDEN, A. J. J. VAN DER & CHESTERS, A. K. 1994*a* An experimental study of the meniscus shape associated with moving liquid-fluid contact lines. *Intl J. Multiphase Flow* **20**, 775.

ZANDEN, A. J. J. VAN DER & CHESTERS, A. K. 1994*b* An approximate solution of the hydrodynamic problem associated with moving liquid–liquid contact lines. *Intl J. Multiphase Flow* **20**, 789.

ZHOU, M.-Y. & SHENG, P. 1990 Dynamics of immiscible-fluid displacement in a capillary tube. *Phys. Rev. Lett.* **64**, 882.